Tailoring Light-Matter Interaction with a Nanoscale Plasmon Resonator

Nathalie P. de Leon,[1,2] Brendan J. Shields,[2] Chun L. Yu,[1] Dirk E. Englund,[2,*] Alexey V. Akimov,[2,3,4] Mikhail D. Lukin,[2,†] and Hongkun Park[1,2,‡]

[1]*Department of Chemistry and Chemical Biology, Harvard University, Cambridge, Massachusetts 02138, USA*
[2]*Department of Physics, Harvard University, Cambridge, Massachusetts 02138, USA*
[3]*Lebedev Institute of Physics, Moscow, Russia*
[4]*Russian Quantum Center, Moscow, Russia*

(Received 3 February 2012; published 31 May 2012)

We propose and demonstrate a new approach for achieving enhanced light-matter interactions with quantum emitters. Our approach makes use of a plasmon resonator composed of defect-free, highly crystalline silver nanowires surrounded by patterned dielectric distributed Bragg reflectors. These resonators have an effective mode volume (V_{eff}) 2 orders of magnitude below the diffraction limit and a quality factor (Q) approaching 100, enabling enhancement of spontaneous emission rates by a factor exceeding 75 at the cavity resonance. We also show that these resonators can be used to convert a broadband quantum emitter to a narrow-band single-photon source with color-selective emission enhancement.

DOI: 10.1103/PhysRevLett.108.226803 PACS numbers: 73.20.Mf, 42.50.Pq, 81.07.Bc, 81.07.Gf

Techniques for controlling light-matter interactions in engineered electromagnetic environments are now being actively explored. Understanding these interactions is not only of fundamental importance but also of interest for applications ranging from optical sensing and metrology to information processing, communication, and quantum science [1–3]. To enhance the coupling between an optical emitter and a desired mode of the radiation field, two approaches can be used [4]. One strategy is to increase the lifetime of the confined optical excitation in high-Q dielectric resonators, such as whispering gallery structures, micropillars, and photonic crystals [3,5]. Another strategy is to reduce the effective mode volume (V_{eff}) of confined radiation [6–9], as is currently explored by using plasmonic nanostructures capable of confining light to dimensions well below the diffraction limit.

Plasmonic resonators, which combine the benefits of both strategies, have potential for engineering light-matter interaction at nanoscales and achieving large coupling between an emitter and the radiation field [2,10]. However, experimental realization of these structures has remained an outstanding challenge [2,11,12]. Prior attempts to control and engineer surface plasmon polariton (SPP) propagation have relied on patterning of metal films using techniques such as focused ion beam and reactive ion etching [13,14]. Unfortunately, these patterning methods introduce defects that act as scattering centers. Moreover, standard metal deposition techniques typically generate polycrystalline films with short SPP propagation lengths. Consequently, plasmonic cavities demonstrated thus far typically had large mode volumes to minimize absorption and scattering in the metal [15–17].

In this Letter, we propose and experimentally demonstrate the new strategy to realize a plasmonic resonator with an exceptionally small mode volume and a moderate Q that can drastically modify the interaction between a quantum emitter and SPPs. In our new approach, illustrated in Fig. 1, we use a patterned dielectric around a plasmonic waveguide to define mirrors and construct a cavity with these mirrors. These cavities exhibit a Q that is limited by intrinsic material absorption rather than fabrication imperfections or the number of mirror slabs. Specifically, our device takes advantage of chemically synthesized silver nanowires (NWs) [18] for tight confinement and reduced group velocity of optical radiation. Owing to their high crystallinity, these NWs support propagation of SPPs over several micrometers in the visible range [16]. We define plasmon distributed Bragg reflectors (DBRs) and cavities by patterning polymethylmethacrylate (PMMA), a low-index dielectric. Unlike patterned metal structures that have been previously employed to manipulate SPP propagation [13–17], patterned PMMA does not suffer from high scattering losses because the relatively low index contrast (compared to metal-air boundaries) reduces susceptibility to lithographic imperfections.

Thin silver NWs surrounded by air support a fundamental SPP mode whose spatial extent is on the order of the wire radius [8]. The effective refractive index for this mode increases when the surrounding medium changes from air to PMMA ($n_{\text{eff}}^{\text{PMMA}} > n_{\text{eff}}^{\text{air}} > 1$), providing the index contrast needed to define DBRs for SPPs. Finite difference-time domain simulations show that a quarter-wave stack composed of several PMMA slabs reflects the incoming SPPs with >90% efficiency [Fig. 1(c)]. The stop band (the wavelength range over which the quarter-wave stack acts as an efficient plasmon mirror) can be tuned over the entire visible range by varying the stack period, with a bandwidth exceeding 100 nm. A sharp resonant feature appears within the stop band when two DBRs are placed together to define a plasmon cavity. Specifically, for a 100 nm diameter NW

 © 2012 American Physical Society

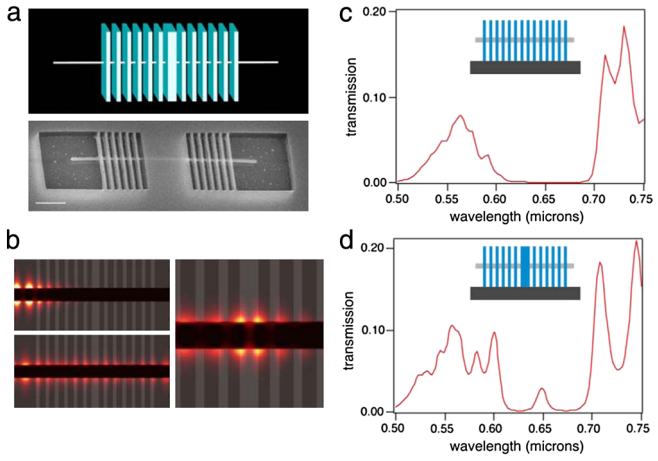

FIG. 1 (color online). (a) Schematic of device concept (top) and scanning electron microscopy image using an Inlens detector (bottom) of the DBR resonator fabricated around a silver NW. The sample is tilted at 30° to demonstrate that the NW is suspended from the substrate in PMMA. Scale bar = 1 μm. (b) Simulated electric field intensity of a plasmonic cavity at wavelengths inside the stop band (top left), outside the stop band (bottom left), and on resonance (right). (c) Simulated transmission spectrum of a DBR consisting of a 100 nm silver NW and PMMA slabs with a period of 200 nm. A quarter-wave stack composed of 6 PMMA slabs reflects the incoming SPPs with a reflectivity exceeding 90%. (d) Simulated transmission spectrum of plasmon cavity composed of two DBRs. The nominal cavity length corresponds to λ_{SPP}, and the linewidth gives a Q of 100.

with DBRs composed of 6 PMMA slabs, a plasmon cavity with $V_{\text{eff}} \sim 0.04(\lambda_0/n)^3$ and $Q \sim 100$ can be achieved [Fig. 1(d); see also Supplemental Material [19]].

When a quantum emitter is placed within this plasmon cavity, its spontaneous emission rate can be dramatically modified. The Purcell factor (F), which is defined as the ratio of the spontaneous emission rates within the cavity (Γ) and in free space (Γ_0), scales as Q/V_{eff} (see Supplemental Material [19]). Equivalently, F can also be expressed as $F_0\mathfrak{T}$, where F_0 and $\mathfrak{T}$ are the Purcell factor of a bare silver NW and the cavity contribution, respectively. We note that $\mathfrak{T}$ is also the finesse of the cavity. For a plasmon cavity with a 100 nm diameter silver NW [Fig. 1(d)], F_0 ranges from 1 to 10 depending on emitter placement [8], and $\mathfrak{T} \sim 20$. F can therefore be as high as 200 when a quantum emitter is placed at the peak electric field of the cavity mode.

Our plasmon resonator architecture offers distinct advantages over other photonic and plasmonic cavity structures [3,15,20,21]. First, the Purcell enhancement achievable in our architecture improves dramatically as the device dimension is pushed well below the diffraction limit [8]. As the NW radius (R) decreases, $V_{\text{eff}} \propto R^3$, while Q can be kept constant by choosing the cavity length to be the half the SPP wavelength. Therefore, the Purcell enhancement also scales as $1/R^3$, indicating that extraordinarily strong coupling can be achieved for small diameter NW devices (see Supplemental Material [19]). This is in stark contrast to dielectric photonic waveguides, in which the field confinement decreases exponentially when the structure dimensions shrink below the diffraction limit [22,23].

In addition, due to its ultrasmall mode volume, our resonator can be used to direct the emission of a broadband quantum emitter into a single cavity mode whose resonant wavelength is selected by the cavity design. When a broadband emitter (e.g., a solid-state emitter with a broad phonon sideband) is coupled to a cavity with a much narrower resonance, the total Purcell factor becomes independent of Q and increases only when V_{eff} is decreased (see Supplemental Material [19]). Therefore, in this broadband emitter regime, ultrasmall mode volume plasmon resonators provide the only means to achieve efficient single-photon sources in which the color of emission can be selected, and the rate into that mode can be enhanced over emission into free space.

We realize the plasmon resonator experimentally by first spin-coating PMMA on a Si/SiO_2 wafer, drop-casting silver NWs, and then spin-coating another layer of PMMA. Electron beam lithography and subsequent development yield suspended NWs in periodic PMMA slabs [Fig. 1(a)] [20,24]. These plasmon DBRs and cavities were characterized via transmission measurements of single nanostructures as a function of wavelength. Because of the wave vector mismatch between propagating SPPs and free space photons, SPPs couple to the far field only at defects or wire ends. We obtain a transmission spectrum by focusing a supercontinuum laser to a diffraction-limited spot at one end of the NW and recording the scattered intensity at the other end as a function of wavelength by using a charge-coupled device (CCD) [Fig. 2(a)].

The data in Fig. 2(b) clearly show that the plasmon DBR exhibits a stop band in transmission, as predicted by the simulations. By comparing the transmission intensity just inside and outside of the stop band (over which range the propagation losses, collection efficiency, and in- and out-coupling efficiencies should be constant; see Supplemental Material [19]), we estimate the reflectivity of the DBR to be 90%–95%. The dropoffs in intensity at shorter and longer wavelengths are due to material absorption and the near-IR cutoff of our optics, respectively.

Transmission spectra of cavities show a peak in the middle of the stop band. In the device shown in Fig. 2(c), the peak is at 638 nm, and the full width at half maximum is 11 nm, corresponding to a Q of 58. The highest Q observed to date in our plasmon cavities is 94, close to the theoretically simulated maximum value. The transmission intensity on resonance is attenuated compared to that outside of the stop band due to higher absorption losses caused by the longer effective path length on resonance, l_{eff}. From the measured value of Q, we determine that l_{eff} is ~ 5 μm (see Supplemental Material [19]). This value is comparable to the SPP propagation length in bare silver

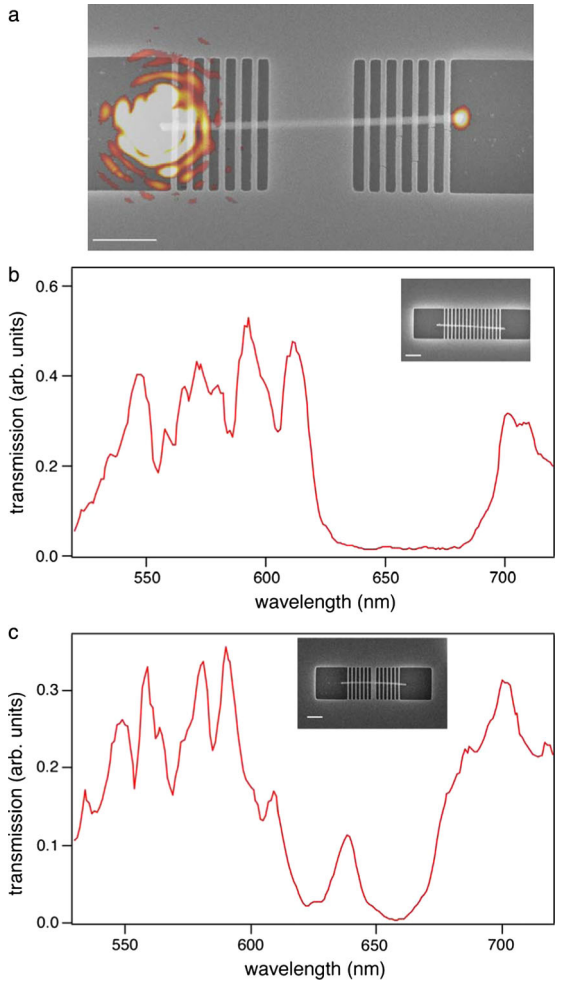

FIG. 2 (color online). (a) CCD image of SPP propagation overlaid on a scanning electron microscopy image of a device. (b) Transmission spectrum of plasmonic DBR. The minimum intensity in the stop band indicates a reflectivity of 90%–95%, and sideband oscillations can be seen outside the stop band. (c) Transmission spectrum of plasmon resonator. The peak in the stop band at 638 nm has a width of 11 nm, corresponding to a Q of 58. Scanning electron microscopy images of both devices are shown in the insets, with scale bars that correspond to 1 μm.

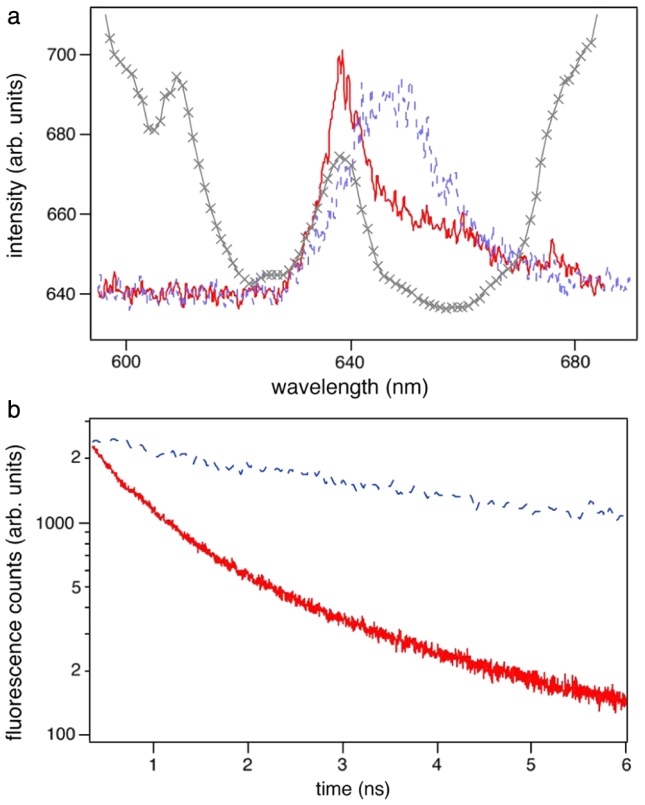

FIG. 3 (color online). (a) Fluorescence spectrum of CdSe quantum dots in the substrate (blue, dashed line) and coupled to the plasmon resonator (red line). The transmission spectrum of the device is overlaid (gray line, crosses). The fluorescence of coupled quantum dots is shifted and narrowed by the cavity resonance. (b) Lifetime measurements obtained by excitation with a pulsed laser of coupled (red line) and uncoupled (blue, dashed line) quantum dots. Uncoupled quantum dots have a lifetime of 16 ns, while coupled quantum dots show multiexponential behavior, with the initial slope corresponding to a lifetime of less than 250 ps.

NWs [25] and indicates that losses in our resonators are dominated by material absorption.

We next demonstrate the utility of our cavities to control both the color and rate of spontaneous emission of solid-state optical emitters. First, we show emission modification in an ensemble of CdSe quantum dots. These quantum dots were coupled to the devices by mixing them homogeneously in PMMA before fabrication. A fluorescence spectrum of the quantum dots coupled to the NW was obtained by exciting one NW end with green light ($\lambda = 532$ nm) and collecting quantum dot fluorescence at the other NW end. Figure 3(a) clearly shows that the plasmon-coupled emission is narrowed and shifted toward the resonance peak when compared to the fluorescence spectrum of uncoupled quantum dots.

The fluorescence lifetime is also modified by the plasmon cavity. The emission from uncoupled quantum dots exhibits a single-exponential decay, characterized by a lifetime (τ_{free}) of 16 ± 3 ns. In contrast, the emission from quantum dots coupled to the NW exhibits a multiexponential decay because the quantum dots are distributed throughout the PMMA, and the detected emission originates from an ensemble of quantum dots along the NW. Notably, the initial slope of this decay yields the shortest lifetime (τ_{coupled}) of less than 250 ps [Fig. 3(b)]. This value suggests that the largest effective Purcell factor $F_{\text{eff}} = \tau_{\text{free}}/\tau_{\text{coupled}}$ is >75, despite the detuning of the cavity resonance relative to the peak of quantum dot emission. It is difficult to disentangle effects of nonradiative decay from lifetime data alone, but we note that quantum dots coupled to a silver NW in unpatterned PMMA show a multiexponential decay with an initial slope corresponding to a lifetime of 4 ns. This evidence indicates that the much shorter lifetime observed in the cavity-coupled decay is

due to radiative emission enhancement rather than nonradiative decay (see Supplemental Material [19]).

We next demonstrate control over emission properties of individual diamond nitrogen vacancy (NV) centers using plasmon resonators. Diamond nanocrystals were coupled to silver NWs by codepositing them during fabrication. Approximately 10% of nanocrystals exhibited the stable, broad fluorescence characteristic of NV centers [Fig. 4(b)] [26]. Once a single NV coupled to the wire was identified, the resonator structure was defined by electron beam lithography around the NV center.

Figure 4(a) shows scanning confocal microscope images of a resonator device with a coupled NV. The top panel shows a reflection image of the device, and the middle panel shows the fluorescence image recorded as the laser is scanned over the device. When the NV is excited (circled), using an independently scanning collection channel (bottom panel) we observe fluorescence from three locations: one corresponding to direct emission from the NV and two corresponding to the ends of the NW. The direct emission from the NV exhibits strongly antibunched autocorrelation [inset in Fig. 4(b)], indicating that it originates from a single NV center. Photon-correlation measurements between the NV fluorescence spot and the NW end also show strong antibunching [inset in Fig. 4(c)], showing that the emission from the wire end also originates from the NV [6,9]. Assuming an SPP out-coupling efficiency of ~5% for these NWs [6,25], we estimate that 50%–60% of the emission couples into SPPs for a typical device.

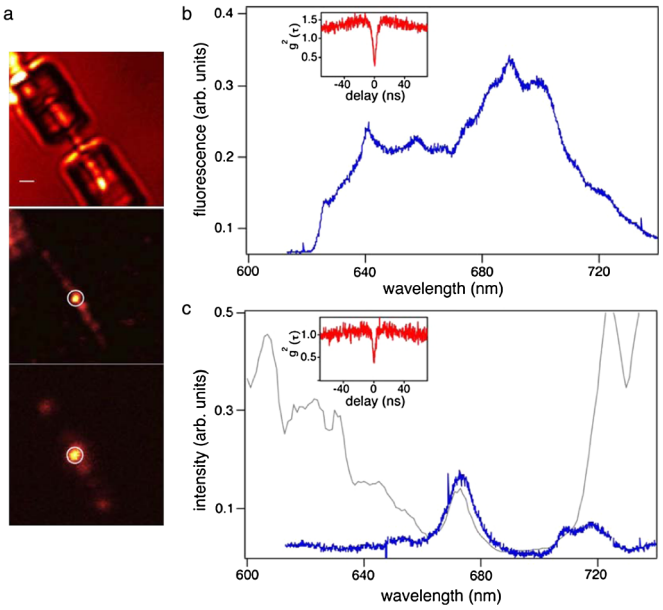

FIG. 4 (color online). (a) Scanning confocal microscope images of the device. The top panel shows an image of the reflected green laser light. The middle panel shows fluorescence in the red as the laser is scanned over the area. When the laser is focused onto the NV in the cavity (indicated with a white circle), an independent collection channel is scanned over the area to detect fluorescence (bottom). The bright spot in the center results from direct excitation and detection of the NV fluorescence. Two additional spots can be seen from the ends of the wire, where SPPs excited by the NV scatter into free space. Scale bar = 1 μm. (b) The fluorescence spectrum from the center of the NW shows broadband emission characteristic of NVs. The inset shows autocorrelation of the fluorescence, which is strongly antibunched, indicating that emission results from a single NV center. (c) The fluorescence spectrum from the end of the NW (red line) shows significant modification, which corresponds to the transmission spectrum of the device (black line). Cross correlation between the SPP-coupled emission and the emission collected directly from the NV indicates that the fluorescence at the end of the NW originates from the same NV center (inset).

The NV fluorescence changes drastically when it is coupled to the plasmon cavity. Before resonator fabrication, the plasmon-coupled NV fluorescence exhibits a broad spectrum spanning a range of 630–740 nm (small, superimposed Fabry-Perot oscillations originate from scattering by the NW ends; see Supplemental Material [19]) [9,16]. After resonator fabrication, the plasmon-coupled NV spectrum exhibits a peak on resonance with the cavity mode and suppressed fluorescence within the stop band [Fig. 4(c)]. The peak position can be placed anywhere across the NV fluorescence spectral range by changing the cavity design, thereby enabling the selection of the wavelength of single-photon emission. The plasmon-coupled fluorescence intensity outside of the stop band ($\lambda > 720$ nm), I_{out}, is essentially unaltered by the cavity and gives the baseline SPP-coupled fluorescence. Notably, the fluorescence intensity on resonance ($\lambda = 637$ nm), I_{res}, is higher than I_{out}. In contrast, the transmission spectrum measured by launching SPPs at the wire end with the supercontinuum laser shows that the transmitted intensity on resonance, T_{res}, is lower than that outside of the stop band, T_{out}.

Comparison of these intensities gives the radiative Purcell enhancement due to the cavity on resonance $\mathfrak{F} = (I_{\mathrm{res}}/I_{\mathrm{out}})(T_{\mathrm{out}}/T_{\mathrm{res}})$; for the device shown, we find that $\mathfrak{F}$ is 11 ± 3. This resonant enhancement is in addition to a broadband enhancement F_0 due to the bare silver NW, which is estimated to be in a range of 1.5–2.5 for NWs of these dimensions [6,9]. Combining these factors together ($F = F_0\mathfrak{F}$), we estimate the overall Purcell enhancement to be as high as 35 at the resonance peak, a value that exceeds the largest Purcell enhancement reported to date for NV centers coupled to dielectric cavities [27,28]. We note that the observed Purcell enhancement is still lower than the theoretical maximum value expected for these devices, most likely because the NV center is not located optimally within the cavity.

The enhanced emitter-cavity coupling observed in the present study can be improved in several ways. Precise placement of NV centers at the peak electric field of the cavity mode would ensure maximum Purcell enhancement for a given device. Furthermore, because the Purcell enhancement scales as $1/R^3$, it can be made substantially higher by using thinner wires [7,8]. In the present study,

we were limited to larger (~100 nm) diameter NWs because we relied on far-field excitation and detection of SPPs. While outcoupling to the far field is less efficient in thinner wires, efficient coupling to thinner NWs can be accomplished with near-field techniques such as evanescently coupled optical fibers [29] and electrical detection [25,30]. Other resonator geometries, such as those that make use of recently developed hyperbolic metamaterials, can potentially be used to further enhance the coupling [31].

The realization of nanoscale plasmon resonators with exceptionally small mode volumes and high quality factors opens new possibilities for integrated plasmonic systems, novel realization of nanoscale lasers and spasers [32], subdiffraction sensing, and optical interfacing of solid-state qubits. For instance, color-selective single-photon sources could have applications in quantum cryptography, and these resonators can be used to direct NV emission into the zero-phonon line for coherent optical manipulation, a crucial requirement for the realization of such applications as single-photon transistors [33]. Other possibilities include high spatial resolution imaging and enhanced coupling of individual molecules. Furthermore, the use of patterned, low-loss dielectrics for controlling SPP propagation in nanoscale plasmonic structures can potentially be extended towards other applications such as plasmonic circuit elements [34,35], outcoupling gratings [11], and metamaterials [36,37].

We acknowledge J. T. Robinson, A. L. Falk, F. Koppens, and J. D. Thompson for helpful discussions. We also gratefully acknowledge support from NSF, DARPA, the Packard Foundation, and the NDSEG.

*Present address: Department of Electrical Engineering, Columbia University, New York, NY 10027, USA.
†To whom correspondence should be addressed.
hongkun_park@harvard.edu
‡lukin@physics.harvard.edu

[1] S. Noda, M. Fujita, and T. Asano, Nature Photon. **1**, 449 (2007).
[2] D. K. Gramotnev and S. I. Bozhevolnyi, Nature Photon. **4**, 83 (2010).
[3] K. Vahala, Nature (London) **424**, 839 (2003).
[4] E. M. Purcell, Phys. Rev. **69**, 681 (1946).
[5] D. Englund, D. Fattal, E. Waks, G. Solomon, B. Zhang, T. Nakaoka, Y. Arakawa, Y. Yamamoto, and J. Vuckovic, Phys. Rev. Lett. **95**, 013904 (2005).
[6] A. V. Akimov, A. Mukherjee, C. L. Yu, D. E. Chang, A. S. Zibrov, P. R. Hemmer, H. Park, and M. D. Lukin, Nature (London) **450**, 402 (2007).
[7] D. E. Chang, A. S. Sorensen, P. R. Hemmer, and M. D. Lukin, Phys. Rev. Lett. **97**, 053002 (2006).
[8] D. E. Chang, A. S. Sorensen, P. R. Hemmer, and M. D. Lukin, Phys. Rev. B **76**, 035420 (2007).
[9] R. Kolesov, B. Grotz, G. Balasubramanian, R. J. Stohr, A. A. L. Nicolet, P. R. Hemmer, F. Jelezko, and J. Wrachtrup, Nature Phys. **5**, 470 (2009).
[10] S. A. Maier, Opt. Quantum Electron. **38**, 257 (2006).
[11] W. L. Barnes, A. Dereux, and T. W. Ebbesen, Nature (London) **424**, 824 (2003).
[12] E. Ozbay, Science **311**, 189 (2006).
[13] B. Wang and G. P. Wang, Appl. Phys. Lett. **87**, 013107 (2005).
[14] M. Sandtke and L. Kuipers, Nature Photon. **1**, 573 (2007).
[15] B. Min, E. Ostby, V. J. Sorger, E. Ulin-Avila, L. Yang, X. Zhang, and K. Vahala, Nature (London) **457**, 455 (2009).
[16] H. Ditlbacher, A. Hohenau, D. Wagner, U. Kreibig, M. Rogers, F. Hofer, F. R. Aussenegg, and J. R. Krenn, Phys. Rev. Lett. **95**, 257403 (2005).
[17] V. J. Sorger, R. F. Oulton, J. Yao, G. Bartal, and X. Zhang, Nano Lett. **9**, 3489 (2009).
[18] B. Wiley, Y. Sun, and Y. Xia, Langmuir **21**, 8077 (2005).
[19] See Supplemental Material at http://link.aps.org/supplemental/10.1103/PhysRevLett.108.226803 for more detailed experimental information and theoretical background.
[20] Y. Zhang and M. Loncar, Opt. Express **16**, 17 400 (2008).
[21] M. Boroditsky, R. Vrijen, T. F. Krauss, R. Coccioli, R. Bhat, and E. Yablonovitch, J. Lightwave Technol. **17**, 2096 (1999).
[22] L. Tong, R. Gattass, J. Ashcom, S. He, J. Lou, M. Shen, I. Maxwell, and E. Mazur, Nature (London) **426**, 816 (2003).
[23] F. Le Kien, S. Dutta Gupta, V. I. Balykin, and K. Hakuta, Phys. Rev. A **72**, 032509 (2005).
[24] C. J. Barrelet, A. B. Greytak, and C. M. Lieber, Nano Lett. **4**, 1981 (2004).
[25] A. L. Falk, F. H. L. Koppens, C. L. Yu, K. Kang, N. d. L. Snapp, A. V. Akimov, M.-H. Jo, M. D. Lukin, and H. Park, Nature Phys. **5**, 475 (2009).
[26] F. Jelezko, C. Tietz, A. Gruber, I. Popa, A. Nizovtsev, S. Kilin, and J. Wrachtrup, Single Mol. **2**, 255 (2001).
[27] T. van der Sar, J. Hagemeier, W. Pfaff, E. C. Heeres, T. H. Oosterkamp, D. Bouwmeester, and R. Hanson, Appl. Phys. Lett. **98**, 193103 (2011).
[28] D. Englund, B. Shields, K. Rivoire, F. Hatami, J. Vuckovic, H. Park, and M. D. Lukin, Nano Lett. **10**, 3922 (2010).
[29] M. Hochberg, T. Baehr-Jones, C. Walker, and A. Scherer, Opt. Express **12**, 5481 (2004).
[30] P. Neutens, P. Van Dorpe, I. De Vlaminck, L. Lagae, and G. Borghs, Nature Photon. **3**, 283 (2009).
[31] Z. Jacob, J.-Y. Kim, G. V. Naik, A. Boltasseva, E. E. Narimanov, and V. M. Shalaev, Appl. Phys. B **100**, 215 (2010).
[32] R. F. Oulton, V. J. Sorger, T. Zentgraf, R.-M. Ma, C. Gladden, L. Dai, G. Bartal, and X. Zhang, Nature (London) **461**, 629 (2009).
[33] D. E. Chang, A. S. Sorensen, E. A. Demler, and M. D. Lukin, Nature Phys. **3**, 807 (2007).
[34] D. Pacifici, H. J. Lezec, and H. A. Atwater, Nature Photon. **1**, 402 (2007).
[35] N. Engheta, A. Salandrino, and A. Alu, Phys. Rev. Lett. **95**, 095504 (2005).
[36] D. R. Smith, J. B. Pendry, and M. C. K. Wiltshire, Science **305**, 788 (2004).
[37] V. Shalaev, Science **322**, 384 (2008).